

Response and Mechanisms of Resistance to Larotrectinib and Selitrectinib in Metastatic Undifferentiated Sarcoma Harboring Oncogenic Fusion of *NTRK1*

Matthew L. Hemming, MD, PhD^{1,2}; Michael J. Nathenson, MD²; Jia-Ren Lin, PhD^{3,4}; Shaolin Mei, MS^{3,4}; Ziming Du, MD, PhD^{3,5}; Karan Malik, BS²; Adrian Marino-Enriquez, MD, PhD⁵; Jyothi P. Jagannathan, MD⁶; Peter K. Sorger, PhD^{3,4,7}; Monica Bertagnoli, MD⁸; Ewa Sicinska, MD⁹; George D. Demetri, MD^{2,4}; and Sandro Santagata, MD, PhD^{3,4,5}

INTRODUCTION

Oncogenic translocations involving the neurotrophic receptor tyrosine kinase genes (*NTRK1*, *NTRK2*, and *NTRK3*), which encode the 3 tropomyosin receptor kinases (TRKs; TRKA, TRKB, and TRKC), produce fusions linking the *NTRK* kinase domain to the transcriptional regulatory elements and upstream coding regions of a variety of genes. These fusions lead to aberrant TRK kinase activity, driving oncogenesis.¹ TRK fusions can be targeted with TRK inhibitors (TRKis), including larotrectinib² and entrectinib,³ which are well tolerated and effective in approximately 75% of patients with *NTRK*-translocated tumors, often producing durable responses.

Acquired resistance to first-generation TRKis arises from secondary mutations within the ATP binding pocket of the kinase domain; these include solvent-front substitutions, gatekeeper mutations, and xDFG-motif substitutions in the activation loop.^{4,5} Second-generation TRKis such as repotrectinib and selitrectinib overcome these resistance mechanisms by contacting different sites within the kinase domain.^{6,7} In a preliminary report, patients with tumors bearing solvent-front substitutions had a response rate of 50% to second-generation TRKis.⁸ Mechanisms of resistance to second-generation TRKis are not well described.

CASE REPORT

A 47-year-old woman presented to an outside hospital with abdominal pain and bloody diarrhea. A rectal mass was identified and resected (Fig 1A; surgery 1 [S1]). A diagnosis of GI stromal tumor was considered, but immunohistochemistry was negative for c-KIT and positive for DOG-1. At the Dana-Farber/Brigham and Women's Cancer Center (DF/BWCC), a diagnosis of unclassified sarcoma, not otherwise specified, was made. Five months later, the patient developed symptomatic locoregional recurrence with liver and lung metastases, which was resected (S2). A *TPM3-NTRK1* fusion was identified using 2 different next-generation

sequencing (NGS) panels (Table 1) and retrospectively identified in S1. The patient was enrolled on a phase II trial (ClinicalTrials.gov identifier: NCT02576431) of larotrectinib (100 mg twice a day), with an initial objective partial response (Figs 1B and 1C). After 6 months on study, restaging scans identified an isolated area of progression in the right hepatic lobe, which was resected (S3), followed by resumption of larotrectinib. NGS from S3 identified an *NTRK1* G595R solvent-front mutation. Three months later, diffuse disease was noted on restaging scans (Fig 1D). An expanded-access, single-patient protocol was initiated using selitrectinib (100 mg twice a day) with dose escalated at cycle 2 to 150 mg twice a day as a result of low plasma drug levels. A partial response was achieved at 3 months, with dramatic reduction in fluorodeoxyglucose uptake within the tumor (Fig 1E). After 5 months, isolated progression of a perihepatic mass was identified and resected (S4). When a second site of progression in the sacrum was identified 1 month later, selitrectinib was increased to 200 mg twice a day with an associated increase in plasma drug levels (Fig 1F). The progressing tumor continued to grow slowly and was resected 3 months later (S5). Selitrectinib was resumed postoperatively, and the patient has remained free of disease progression for > 1 year.

MATERIALS AND METHODS

Informed Consent

Patients provided informed consent for these institutional review board–approved studies and correlative analyses. We obtained all permissions required by law and the DF/BWCC for publication.

Tumor Sequencing and Analysis

Targeted NGS was performed using the DF/BWCC OncoPanel⁹ or FoundationOne Heme (Foundation Medicine, Cambridge, MA) to assess > 400 cancer-associated genes and select translocations. RNA-seq using single-end 75–base pair reads was performed as previously described.¹⁰ Fastq files were aligned to

ASSOCIATED CONTENT

Appendix
Author affiliations and support information (if applicable) appear at the end of this article.

Accepted on December 13, 2019 and published at ascopubs.org/journal/po on February 14, 2020; DOI <https://doi.org/10.1200/P0.19.00287>

Creative Commons Attribution Non-Commercial No Derivatives 4.0 License



CONTEXT

Key Objective

Mechanisms of resistance to second-generation tropomyosin receptor kinase (TRK) inhibitors are not well described.

Knowledge Generated

In this case report, we identified a gain-of-function *KRAS* mutation resulting in signal transduction pathway reactivation and associated tumor progression despite continuous TRK inhibitor therapy. Changes in the tumor microenvironment were identified, consisting of a significant increase in cytotoxic T cells and macrophages.

Relevance

These findings help define mechanisms of resistance to second-generation TRK inhibitors and suggest novel strategies to treat resistant disease.

hg19 using STAR,¹¹ and expression was quantified using Cufflinks.¹² Gene set enrichment analysis (GSEA)¹³ was performed using the Hallmark, KEGG, or Reactome databases. Data are publicly available (GSE132439). GUARDANT360 (Guardant Health, Redwood City, CA) circulating tumor DNA (ctDNA) sequencing was also performed.

Multiplexed Immunofluorescence

Tissue-based cyclic immunofluorescence (CyCIF) was performed on formalin-fixed paraffin-embedded specimens, as previously described,¹⁴ using qualified antibodies¹⁵ listed in Appendix Table A1 and uploaded to cycif.org.

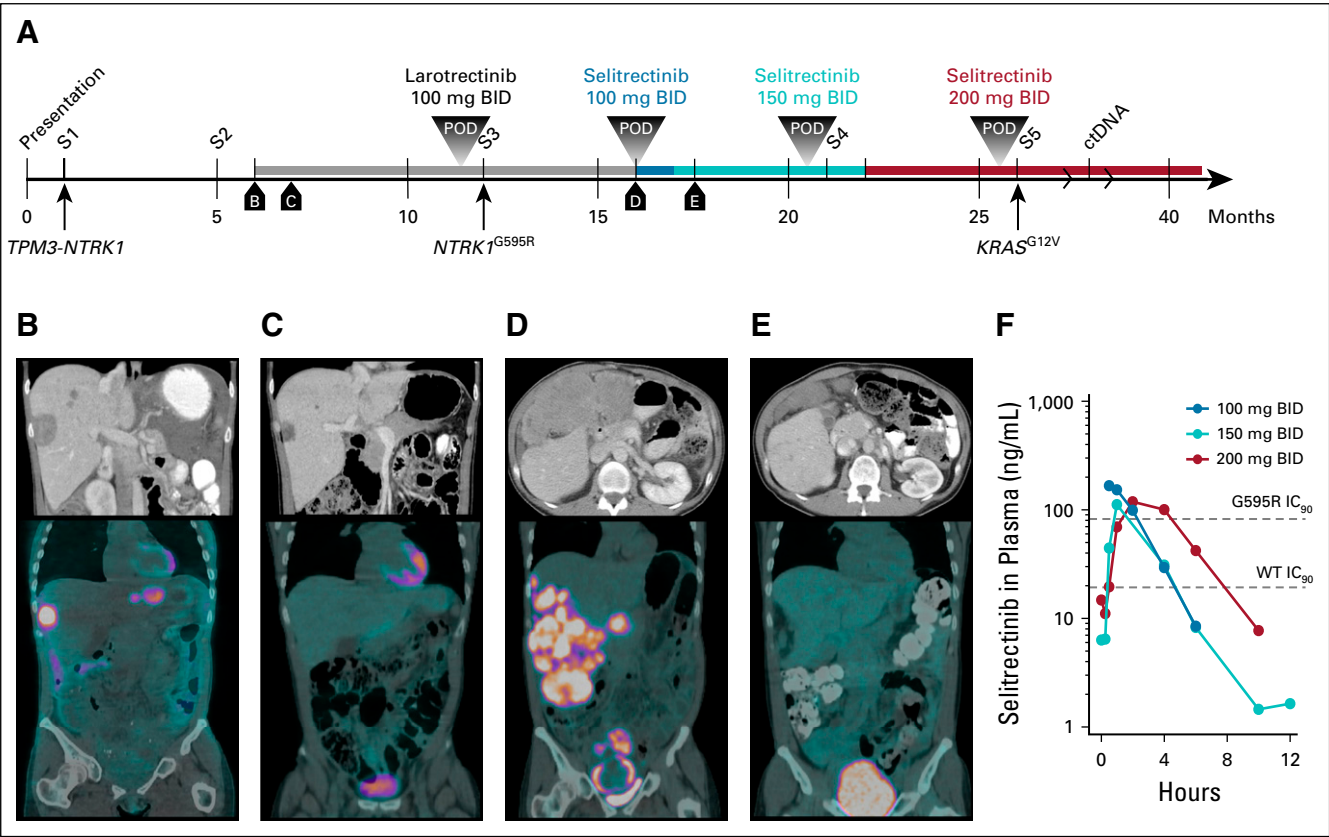


FIG 1. Treatment timeline and assessments. (A) Timeline of diagnosis and therapeutic interventions. Surgeries are numbered sequentially, and boxed lettering indicates the time of computed tomography (CT) and positron emission tomography (PET)-CT imaging. (B-E) Contrast-enhanced CT scans (top panels) and PET-CT images (bottom panels) from patient staging scans as indicated on the timeline. (F) Plasma levels over time of selitrectinib at the indicated dose levels. Data from each dosing point are derived from cycle 1, day 1 pharmacokinetic studies. Dashed lines indicating the 90% inhibitory concentration (IC₉₀) of wild-type (WT) and G595R-mutant *TRKA* are shown. BID, twice a day; ctDNA, circulating tumor DNA; POD, progression of disease; S, surgery.

TABLE 1. Diagnosis, Treatment, and NGS Testing

Surgery No.	Procedure	Pathologic Interpretation	Systemic Treatment	NGS Platform	Results
S1	LAR of primary rectal tumor, TAH+BS	Original diagnosis: GIST with predominantly epithelioid and focal spindle cell features Revised diagnosis: Malignant epithelioid and spindle cell neoplasm: unclassified sarcoma	None	FoundationOne Heme (Foundation Medicine, Cambridge, MA)	<i>TPM3-NTRK1</i> fusion, <i>PTEN</i> truncation TMB = 2.94
S2	Resection of symptomatic pelvic recurrence	Malignant epithelioid and spindle cell neoplasm: unclassified sarcoma with myxoid features	None	Paradigm (Paradigm Diagnostics, Phoenix, AZ) OncoPanel (Dana-Farber Cancer Institute and Brigham and Women's Hospital, Boston, MA)	<i>TPM3-NTRK1</i> fusion <i>NTRK1</i> fusion, <i>PTEN-STAT3</i> fusion VUS: <i>EP300</i> , <i>PBRM1</i> , <i>RB1</i> , <i>ZNF217</i>
S3	Resection of progressive right liver mass	Metastatic epithelioid and spindle cell sarcoma with myxoid features	Larotrectinib 100 mg twice a day	FoundationOne Heme OncoPanel	<i>TPM3-NTRK1</i> fusion, <i>NTRK1</i> G595R, <i>PTEN</i> truncation VUS: <i>NCOR2</i> fs TMB = 6 <i>TPM3-NTRK1</i> fusion, <i>NTRK1</i> G595R, <i>PTEN-STAT3</i> fusion VUS: <i>EP300</i> , <i>PBRM1</i> , <i>RB1</i> , <i>ZNF217</i>
S4	Resection of progressive perihepatic mass	Metastatic epithelioid and spindle cell sarcoma; multiple areas with necrosis and hyalinization; the growing nodule had < 5% treatment effect	Selitrectinib 150 mg twice a day	FoundationOne Heme OncoPanel	<i>TPM3-NTRK1</i> fusion, <i>NTRK1</i> G595R, <i>PTEN</i> truncation VUS: <i>PTCH1</i> fs TMB = 4 <i>TPM3-NTRK1</i> fusion, <i>NTRK1</i> G595R, <i>PTEN-STAT3</i> fusion VUS: <i>PTCH1</i> fs, <i>EP300</i> , <i>PBRM1</i> , <i>RB1</i> , <i>ZNF217</i> TMB = 4.5
S5	Resection of progressive presacral mass cDNA	Metastatic epithelioid and spindle cell sarcoma; areas of moderate to complete necrosis and hyalinization	Selitrectinib 200 mg twice a day	FoundationOne Heme Guardant (Guardant Health, Redwood City, CA)	<i>TPM3-NTRK1</i> fusion, <i>NTRK1</i> G595R, <i>PTEN</i> truncation, <i>KRAS</i> G12V VUS: <i>PTCH1</i> fs TMB = 5 <i>NTRK1</i> fusion, <i>NTRK1</i> G595R, <i>KRAS</i> G12V cDNA undetectable

Abbreviations: cDNA, circulating tumor DNA; GIST, GI stromal tumor; LAR, low anterior resection; NGS, next-generation sequencing; TAH+BS, total abdominal hysterectomy with bilateral salpingectomy; TMB, tumor mutational burden in mutations per megabase; VUS, variant of uncertain significance.

Patient-Derived Models

Tumor was implanted subcutaneously into female nude mice (NU/NU; Charles River Laboratories, Wilmington, MA) to produce patient-derived xenografts (PDXs) following protocols approved by the institution's Institutional Animal Care and Use Committee. Primary cultures were established by generating a tumor suspension and passaging adherent cells.

RESULTS

To explore resistance mechanisms to second-generation TRKis, we performed targeted NGS of inhibitor-sensitive and -resistant tumors. Compared with S3, which was sensitive to selitrectinib, S4 harbored a *PTCH1* frameshift mutation (Table 1). *PTCH1* normally functions as a tumor suppressor,¹⁶ and its inactivation promotes Hedgehog signaling. In addition to the *PTCH1* mutation, S5 also harbored a *KRAS* G12V mutation and variants of unknown significance (Table 1). ctDNA sequencing after S5 failed to detect *NTRK* fusions or known tumor mutations. All sequenced tumors exhibited a likely inactivating *PTEN* rearrangement.

To characterize potential transcriptional mechanisms underlying selitrectinib resistance, we analyzed S3 and S5 by RNA-seq. A tumor from a separate patient with an *ETV6-NTRK3* translocated sarcoma was also analyzed. Compared with the *ETV6-NTRK3* tumor, all *TPM3-NTRK1* tumors exhibited exclusive expression of *NTRK1* exons associated with the oncogenic fusion (Fig 2A). Similar findings were observed in a cell line and PDX generated from S3 and S5 (Appendix Fig A1A). Although all samples expressed *TPM3* and *ETV6*, only the *ETV6-NTRK3* tumor expressed detectable *NTRK3* transcript (Fig 2B). The S5 tumor treated with selitrectinib expressed lower levels of the *TPM3-NTRK1* fusion transcript (Fig 2B). Using GSEA to explore pathways associated with selitrectinib resistance, the S5 tumor exhibited enrichment in *KRAS*-related signaling as compared with the S3 tumor (Fig 2C), consistent with oncogenic activation of *KRAS* signaling. An inflammatory response signature was similarly enriched in S5 compared with S3 (Fig 2D), and these gene sets showed similar enrichment in PDXs (Appendix Figs A1B and A1C). Through GSEA comparisons of multiple databases, S5 showed recurrent enrichment of immune- and inflammatory-related signatures as compared with S3 (Fig 2E). To further characterize the inflammatory infiltrate, we performed CIBERSORT analysis¹⁷; this showed that M1 macrophages and CD8 T-cell subsets were enriched in the S5 tumor (Fig 2F). Consistent with this analysis, levels for several markers of T cells (CD8A and CD3), T-cell activation (CD48), macrophages (CD68), and several modulators of the immune microenvironment¹⁸ were higher in S5 (Fig 2G). Despite the loss-of-function mutation in *PTCH1*, we found no evidence of activation of the Hedgehog signaling pathway by RNA-seq (Appendix Figs A2A and A2B).

To further characterize the tumor microenvironment and its organization, we performed multiplexed immunofluorescence imaging (CyCIF)¹⁴ of S2, S3, and S5 followed by single-cell analysis. All tumors stained positive for TRK, with evidence of inflammatory infiltrates in S3 and S5 (Fig 3A). Compared with S2, S3 and, to a greater extent, S5 had a higher density of CD45⁺ immune cells including cytotoxic T cells and CD68⁺ macrophages (Fig 3B). Infiltration by these immune cells was significantly greater in S5, in agreement with transcriptional profiling results. Spatial neighborhood analysis showed that S5 had more CD68⁺ macrophages and CD8a⁺ T cells surrounding tumor cells as compared with S3 (Figs 3C to 3E, Appendix Fig A3). Moreover, spatial analysis revealed a higher density of interfacing programmed cell death 1 (PD-1)-positive and programmed death ligand 1 (PD-L1)-positive cells in S3 than S5 (Fig 3F-G).

DISCUSSION

We report here a patient with a *TPM3-NTRK1*-driven sarcoma that developed resistance to first- and second-generation TRKis. The tumor initially developed resistance to larotrectinib through an *NTRK1* solvent-front mutation; resistance was overcome with the second-generation TRKi selitrectinib. Two sites of focal progression were surgically resected while on selitrectinib. No clear secondary oncogenic mutation was identified in S4, and the dose of selitrectinib was increased to 200 mg twice a day. Isolated progression was observed at the high drug dose, the tumor was resected (S5), and the gain-of-function *KRAS* G12V mutation was identified. Transcriptional profiling was consistent with functional activation of *KRAS* signaling in this tumor.

Dysregulation of *KRAS* signaling in an *NTRK* fusion-driven sarcoma initially treated with effective TRKis is analogous to the well-characterized mechanism of acquired anti-epidermal growth factor receptor (EGFR) antibody resistance in colorectal cancer. In a subset of these tumors, *KRAS* mutations emerge to drive resistance to EGFR inhibition through reactivation of oncogenic signaling.^{19,20} We speculate that consequent reactivation of signal transduction pathways by mutant *KRAS* overcomes effective inhibition of the *NTRK* fusion oncogene. Elevated levels of TRK protein in S5 relative to S3 despite lower expression of the fusion transcript may further suggest effective TRK inhibition because kinase inhibition can stabilize kinase conformation, decrease protein turnover, and prolong half-life.^{21,22}

Although the etiology of the increased inflammatory infiltrate in the *KRAS* G12V mutant tumor (S5) is unclear, evidence from other cancer types suggests that *KRAS* mutations may alter the immune microenvironment.^{23,24} Several targets of immuno-oncology therapies were expressed at higher levels in S5, suggesting an alternative means of targeting resistant disease (although the number

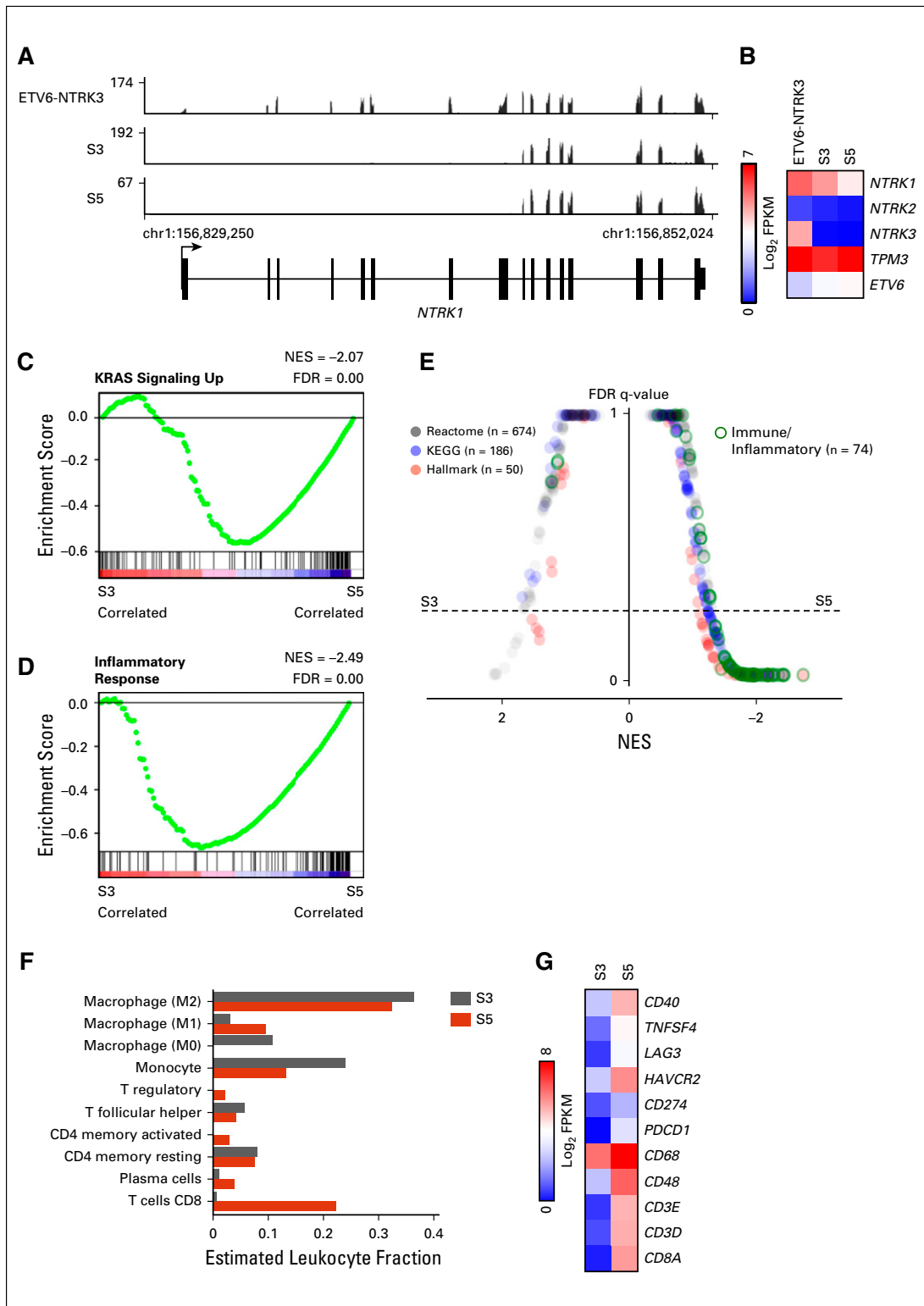


FIG 2. Expression profiling of selitrectinib-sensitive and -resistant samples. (A) Plot of mapped RNA-seq reads at the *NTRK1* locus for an ETV6-NTRK3 tumor and TPM3-NTRK1 tumors from surgery (S) 3 and S5. (B) Heatmap of RNA-seq data demonstrating expression of *NTRK* genes and fusion partners. (C and D) Hallmark gene sets for KRAS signaling up and inflammatory response comparing S3 and S5. (E) Butterfly plot of all Reactome, KEGG, and Hallmark gene sets (n = 910) comparing S3 and S5 tumors. Immune and inflammatory gene sets are outlined in green. (F) CIBERSORT analysis of S3 and S5 tumors showing relative leukocyte abundance. Cell types with nonzero leukocyte fraction are shown. (G) Heatmap showing relative expression of select immune-related genes. FDR, false discovery rate; NES, normalized enrichment score.

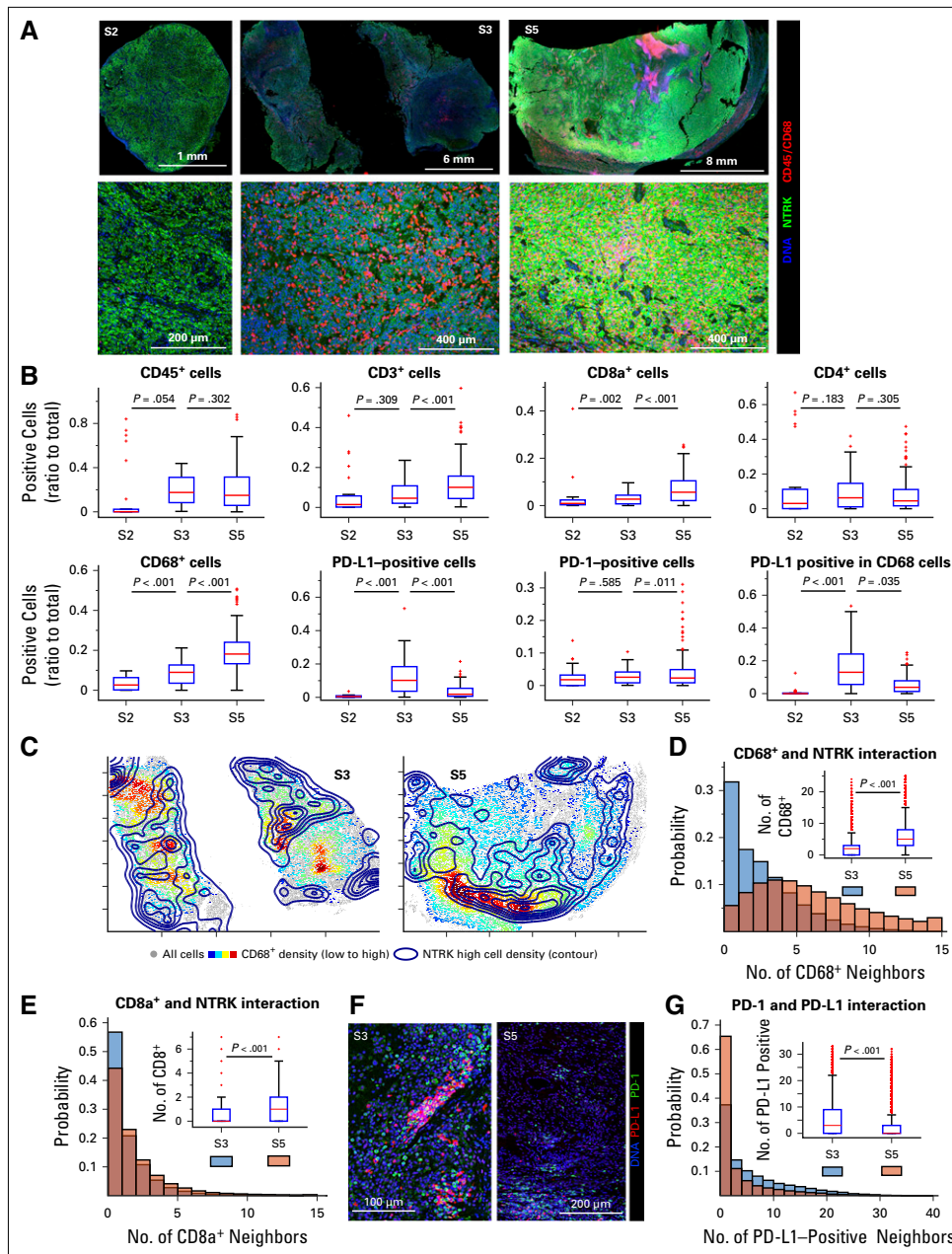


FIG 3. Multiplexed imaging of the immune microenvironment in serial tumor resections. (A) Tissue-based cyclic immunofluorescence images from surgery (S) 2, S3, and S5 samples demonstrating staining for tropomyosin receptor kinase (TRK), CD45, and CD68, with lower panels representing magnified images of the upper panels. (B) Immune cell counts, with digital images from the indicated single or multiplexed antibodies processed as previously described.¹⁴ Cell counts were calculated frame by frame and are represented as box plots, with the median indicated in red. (C) Global distribution of cells staining highest for TRK (contour map) and CD68⁺ cells (heatmap, with red indicating higher cell density) in S3 and S5. (D and E) Histograms representing the number of CD68⁺ or CD8a⁺ cells neighboring TRK^{high} cells. Cumulative probabilities in each imaged frame are shown as a box plot (inset). (F) Representative staining of programmed cell death 1 (PD-1) and programmed death ligand 1 (PD-L1) in samples S3 and S5, respectively. (G) Proximity probability of cells staining positive for PD-1 and PD-L1, with histogram representing the number of PD-L1-positive cells neighboring PD-1-positive cells. Cumulative probabilities in each imaged frame are shown as a box plot (inset). A two-sample *t* test was used to compare groups, with *P* values indicated; the frame numbers in each sample are 33 (S2), 127 (S3), and 168 (S5).

of cells expressing PD-1 and PD-L1 protein was discordant with RNA expression, as has been observed elsewhere²⁵. Furthermore, data from colorectal carcinoma suggests an association between kinase fusions and response to checkpoint inhibitor therapy,²⁶ suggesting the rational combination of TRKis and immuno-oncology therapeutics for resistant disease.

As exemplified by this patient, treatment with second-generation TRKis can elicit durable response⁸; the patient remains well > 1 year on selitrectinib after the final resection. Imaging using [¹⁸F]fluorodeoxyglucose positron emission tomography may be a useful early marker of

effective TRK inhibition and tumor response. Consistent with our findings on reactivation of the mitogen-activated protein kinase (MAPK) pathway as a mechanisms of TRKi resistance, alterations in *BRAF*, *KRAS*, and *MET* were recently reported to confer resistance to second-generation TRKis in carcinomas, with clinical benefit derived from targeting the reactivated signal transduction pathways.^{27,28} These results provide insight into mechanisms of pathway reactivation under conditions of continued TRK inhibition and identify changes in the immune microenvironment that may play important roles in the diagnosis and treatment of resistant disease.

AFFILIATIONS

¹Department of Medical Oncology, Dana-Farber Cancer Institute, Boston, MA

²Center for Sarcoma and Bone Oncology, Dana-Farber Cancer Institute, Harvard Medical School, Boston, MA

³Laboratory of Systems Pharmacology, Harvard Medical School, Boston, MA

⁴Ludwig Center at Harvard, Boston, MA

⁵Department of Pathology, Brigham and Women's Hospital, Harvard Medical School, Boston, MA

⁶Department of Imaging, Dana-Farber Cancer Institute, Harvard Medical School, and Department of Radiology, Brigham and Women's Hospital, Boston, MA

⁷Department of Systems Biology, Harvard Medical School, Boston, MA

⁸Department of Surgery, Brigham and Women's Hospital, Harvard Medical School, Boston, MA

⁹Department of Oncologic Pathology, Dana-Farber Cancer Institute, Harvard Medical School, Boston, MA

Collection and assembly of data: Matthew L. Hemming, Michael

J. Nathenson, Jia-Ren Lin, Shaolin Mei, Karan Malik, Adrian Marino-Enriquez, Ewa Sicinska, George D. Demetri

Data analysis and interpretation: Matthew L. Hemming, Michael J. Nathenson, Jia-Ren Lin, Shaolin Mei, Ziming Du, Adrian Marino-Enriquez, Jyothi P. Jagannathan, Monica Bertagnolli, George D. Demetri, Sandro Santagata

Manuscript writing: All authors

Final approval of manuscript: All authors

Accountable for all aspects of the work: All authors

AUTHORS' DISCLOSURES OF POTENTIAL CONFLICTS OF INTEREST

The following represents disclosure information provided by authors of this manuscript. All relationships are considered compensated unless otherwise noted. Relationships are self-held unless noted. I = Immediate Family Member, Inst = My Institution. Relationships may not relate to the subject matter of this manuscript. For more information about ASCO's conflict of interest policy, please refer to www.asco.org/rwc or ascopubs.org/po/author-center.

Open Payments is a public database containing information reported by companies about payments made to US-licensed physicians ([Open Payments](http://OpenPayments)).

Peter K. Sorger

Leadership: RareCyte, Merrimack, Applied BioMath

Stock and Other Ownership Interests: RareCyte, Merrimack Pharma, Applied BioMath, Glencoe Software

Honoraria: Novartis

Research Funding: Merck (Inst)

Monica Bertagnolli

Research Funding: AbbVie (Inst), Agenus (Inst), Astellas Pharma (Inst), AstraZeneca (Inst), Breast Cancer Research Foundation (Inst), Bristol-Myers Squibb (Inst), Celgene (Inst), Complion (Inst), Exelixis (Inst), Genentech (Inst), GHI Pharma (Inst), Gilead Sciences (Inst), GlaxoSmithKline (Inst), Incyte (Inst), Jazz Pharmaceuticals (Inst), Leidos (Inst), Eli Lilly (Inst), Matrex (Inst), Mayo Clinic (Inst), MGH (Inst), Millennium Pharmaceuticals (Inst), Novartis (Inst), Patient-Centered Outcomes Research Institute (PCORI) (Inst), Pfizer (Inst), Robert Wood Johnson Foundation (Inst), Sagerock Advisors (Inst), Taiho Pharmaceutical (Inst), Bayer Health (Inst), Eisai (Inst), Leidos (Inst), Lexicon (Inst), Merck (Inst), Pharmacocyclics (Inst), Takeda (Inst), Tesaro (Inst), Baxalta (Inst), Sanofi (Inst), Teva (Inst), Janssen (Inst), Merck (Inst)

Uncompensated Relationships: Leap Therapeutics, Syntimmune, Syntalogic

CORRESPONDING AUTHOR

George D. Demetri, MD, Dana-Farber Cancer Institute, 450 Brookline Ave, Boston, MA 02215; e-mail: george_demetri@dfci.harvard.edu.

EQUAL CONTRIBUTION

M.L.H., M.J.N., and J-R.L. contributed equally to this work. S.S. and G.D.D. contributed equally to this work.

SUPPORT

Supported by National Institutes of Health (NIH) Grant No. U54-CA225088 (P.K.S. and S.S.), Harvard Catalyst Medical Research Investigator Training Program NIH Award No. UL 1TR002541 (M.L.H.), Brigham and Women's Hospital Program in Precision Medicine (A.M.E.), and the Ludwig Center at Harvard (P.K.S., S.S., and G.D.D.).

AUTHOR CONTRIBUTIONS

Conception and design: Matthew L. Hemming, Michael J. Nathenson, Jia-Ren Lin, Shaolin Mei, Peter K. Sorger, George D. Demetri, Sandro Santagata

Financial support: Matthew L. Hemming, Peter K. Sorger, George D. Demetri, Sandro Santagata

Administrative support: Peter K. Sorger, Sandro Santagata

Provision of study materials or patients: Matthew L. Hemming, Peter K. Sorger, Monica Bertagnolli, Ewa Sicinska, George D. Demetri, Sandro Santagata

Open Payments Link: <https://openpaymentsdata.cms.gov/physician/114497/summary>

George D. Demetri

Leadership: Blueprint Medicines, Merrimack

Stock and Other Ownership Interests: Blueprint Medicines, G1 Therapeutics, Bessor Pharma, Caris Life Sciences, Champions Oncology, Merrimack, Erasca

Consulting or Advisory Role: Bayer, Pfizer, Novartis, EMD Serono, Sanofi, Janssen Oncology, PharmaMar, Daiichi Sankyo, Blueprint Medicines, WIRB-Copernicus Group, ZIOPHARM Oncology, Polaris, G1 Therapeutics, Caris Life Sciences, Adaptimmune, Ignyta, Genentech, Loxo, Mirati Therapeutics, M.J. Hennessey/OncLive, Medscape, ICON Clinical Research

Research Funding: AbbVie (Inst), Janssen Oncology (Inst), Bayer (Inst), Novartis (Inst), Pfizer (Inst), Ignyta (Inst), Genentech (Inst), Loxo (Inst), AbbVie (Inst), Epizyme (Inst), Adaptimmune (Inst), GlaxoSmithKline (Inst)

Patents, Royalties, Other Intellectual Property: Patent on use of imatinib for GI stromal tumor, receive minor royalty payment from Dana-Farber after license between Dana-Farber and Novartis.

Sandro Santagata

Consulting or Advisory Role: RareCyte

Patents, Royalties, Other Intellectual Property: US9696313B2 (HSF1 as a marker in tumor prognosis and treatment), US20150241436A1 (Hsf1 and hsf1 cancer signature set genes and uses relating thereto), US20170037480A1 (Hsf1 in tumor stroma), US20170037480A1 (Hsf1 in tumor stroma), US20180306796A1 (Methods and compositions relating to proteasome inhibitor resistance), Combination Treatments of Hsp90 Inhibitors for Enhancing Tumor Immunogenicity and Methods of Use Thereof (application pending), Targeted Manipulation of the Proteasome Subunit Expression Levels as a Method for Curing Cancer (application pending).

No other potential conflicts of interest were reported.

ACKNOWLEDGMENT

We thank LOXO Oncology for providing pharmacokinetic data.

REFERENCES

- Amatu A, Sartore-Bianchi A, Siena S: *NTRK* gene fusions as novel targets of cancer therapy across multiple tumour types. *ESMO Open* 1:e000023, 2016
- Drilon A, Laetsch TW, Kummar S, et al: Efficacy of larotrectinib in *TRK* fusion-positive cancers in adults and children. *N Engl J Med* 378:731-739, 2018
- Drilon A, Siena S, Ou SI, et al: Safety and antitumor activity of the multitargeted pan-*TRK*, *ROS1*, and *ALK* inhibitor entrectinib: Combined results from two phase I trials (ALKA-372-001 and STARTRK-1). *Cancer Discov* 7:400-409, 2017
- Russo M, Misale S, Wei G, et al: Acquired resistance to the *TRK* inhibitor entrectinib in colorectal cancer. *Cancer Discov* 6:36-44, 2016
- Cocco E, Scaltriti M, Drilon A: *NTRK* fusion-positive cancers and *TRK* inhibitor therapy. *Nat Rev Clin Oncol* 15:731-747, 2018
- Drilon A, Nagasubramanian R, Blake JF, et al: A next-generation *TRK* kinase inhibitor overcomes acquired resistance to prior *TRK* kinase inhibition in patients with *TRK* fusion-positive solid tumors. *Cancer Discov* 7:963-972, 2017
- Drilon A, Ou SI, Cho BC, et al: Repotrectinib (TPX-0005) is a next-generation *ROS1/TRK/ALK* inhibitor that potently inhibits *ROS1/TRK/ALK* solvent-front mutations. *Cancer Discov* 8:1227-1236, 2018
- Hyman D, Kummar S, Farago AF, et al: Phase I and expanded access experience of LOXO-195 (BAY 2731954), a selective next-generation *TRK* inhibitor (*TRKi*). *Cancer Res* 79, 2019 (abstr CT127)
- Garcia EP, Minkovsky A, Jia Y, et al: Validation of OncoPanel: A targeted next-generation sequencing assay for the detection of somatic variants in cancer. *Arch Pathol Lab Med* 141:751-758, 2017
- Hemming ML, Lawlor MA, Zeid R, et al: Gastrointestinal stromal tumor enhancers support a transcription factor network predictive of clinical outcome. *Proc Natl Acad Sci USA* 115:E5746-E5755, 2018
- Dobin A, Davis CA, Schlesinger F, et al: STAR: Ultrafast universal RNA-seq aligner. *Bioinformatics* 29:15-21, 2013
- Trapnell C, Williams BA, Pertea G, et al: Transcript assembly and quantification by RNA-Seq reveals unannotated transcripts and isoform switching during cell differentiation. *Nat Biotechnol* 28:511-515, 2010
- Subramanian A, Tamayo P, Mootha VK, et al: Gene set enrichment analysis: A knowledge-based approach for interpreting genome-wide expression profiles. *Proc Natl Acad Sci USA* 102:15545-15550, 2005
- Lin J-R, Izar B, Wang S, et al: Highly multiplexed immunofluorescence imaging of human tissues and tumors using t-CyCIF and conventional optical microscopes. *eLife* 7:545, 2018
- Du Z, Lin J-R, Rashid R, et al: Qualifying antibodies for image-based immune profiling and multiplexed tissue imaging. *Nat Protoc* 14:2900-2930, 2019
- Pan S, Dong Q, Sun LS, et al: Mechanisms of inactivation of *PTCH1* gene in nevoid basal cell carcinoma syndrome: Modification of the two-hit hypothesis. *Clin Cancer Res* 16:442-450, 2010
- Newman AM, Liu CL, Green MR, et al: Robust enumeration of cell subsets from tissue expression profiles. *Nat Methods* 12:453-457, 2015
- Marshall HT, Djamgoz MBA: Immuno-oncology: Emerging targets and combination therapies. *Front Oncol* 8:315, 2018
- Misale S, Yaeger R, Hobor S, et al: Emergence of *KRAS* mutations and acquired resistance to anti-EGFR therapy in colorectal cancer. *Nature* 486:532-536, 2012
- Zhao B, Wang L, Qiu H, et al: Mechanisms of resistance to anti-EGFR therapy in colorectal cancer. *Oncotarget* 8:3980-4000, 2017
- Miyazawa K, Toyama K, Gotoh A, et al: Ligand-dependent polyubiquitination of c-kit gene product: A possible mechanism of receptor down modulation in M07e cells. *Blood* 83:137-145, 1994
- Scaltriti M, Verma C, Guzman M, et al: Lapatinib, a *HER2* tyrosine kinase inhibitor, induces stabilization and accumulation of *HER2* and potentiates trastuzumab-dependent cell cytotoxicity. *Oncogene* 28:803-814, 2009
- Dias Carvalho P, Guimarães CF, Cardoso AP, et al: *KRAS* oncogenic signaling extends beyond cancer cells to orchestrate the microenvironment. *Cancer Res* 78:7-14, 2018
- Liao W, Overman MJ, Boutin AT, et al: *KRAS-IRF2* axis drives immune suppression and immune therapy resistance in colorectal cancer. *Cancer Cell* 35:559-572.e7, 2019

25. Coppock JD, Volaric AK, Mills AM, et al: Concordance levels of PD-L1 expression by immunohistochemistry, mRNA in situ hybridization, and outcome in lung carcinomas. *Hum Pathol* 82:282-288, 2018
 26. Cocco E, Benhamida J, Middha S, et al: Colorectal carcinomas containing hypermethylated MLH1 promoter and wild-type BRAF/KRAS are enriched for targetable kinase fusions. *Cancer Res* 79:1047-1053, 2019
 27. Cocco E, Schram AM, Kulick A, et al: Resistance to TRK inhibition mediated by convergent MAPK pathway activation. *Nat Med* 25:1422-1427, 2019
 28. Doebele RC: Acquired resistance is oncogene and drug agnostic. *Cancer Cell* 36:347-349, 2019
-

APPENDIX

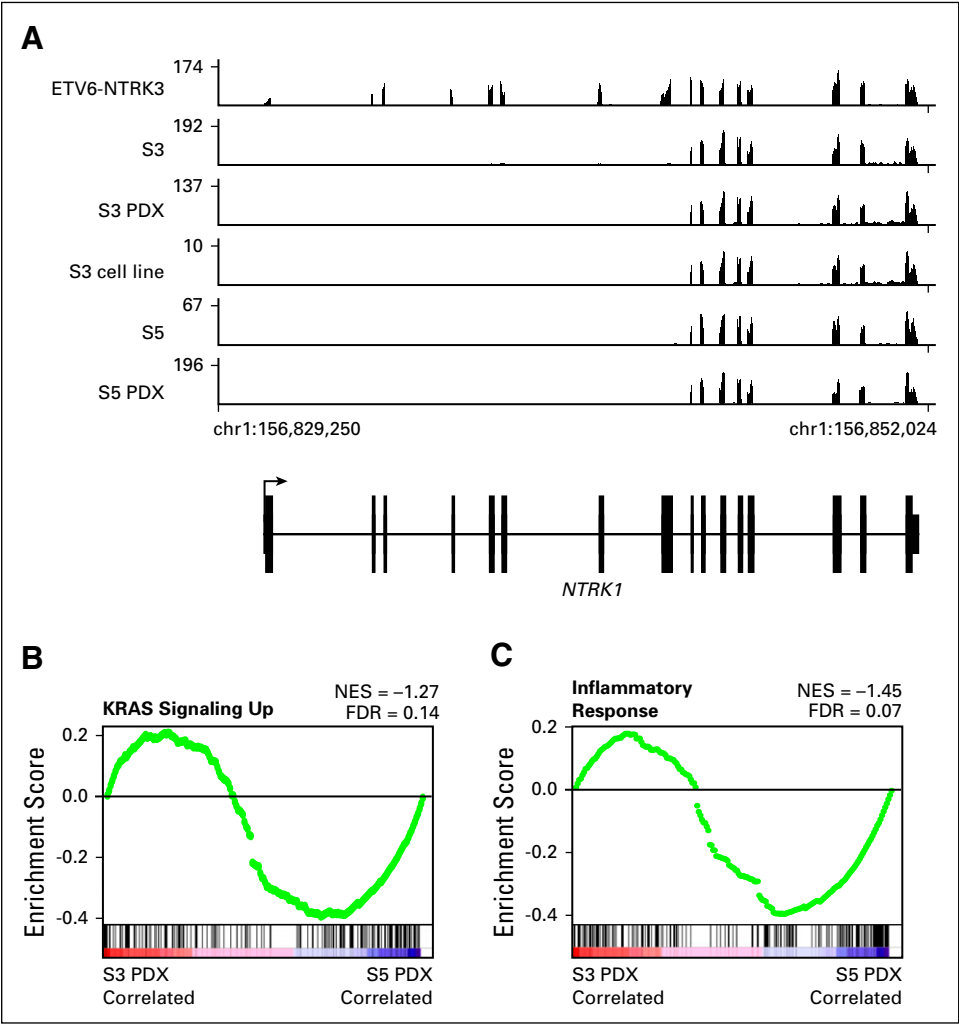


FIG A1. Expression profiling of NTRK translocated models. (A) Plot of mapped RNA-seq reads at the *NTRK1* locus for an ETV6-NTRK3 tumor and TPM3-NTRK1 tumors from surgery (S) 3, S3 patient-derived xenograft (PDX), S3 cell line, S5, and S5 PDX. (B and C) Hallmark gene set for *KRAS* signaling up and inflammatory response comparing S3 and S5 PDX grown in athymic, T-cell-deficient mice. FDR, false discovery rate; NES, normalized enrichment score.

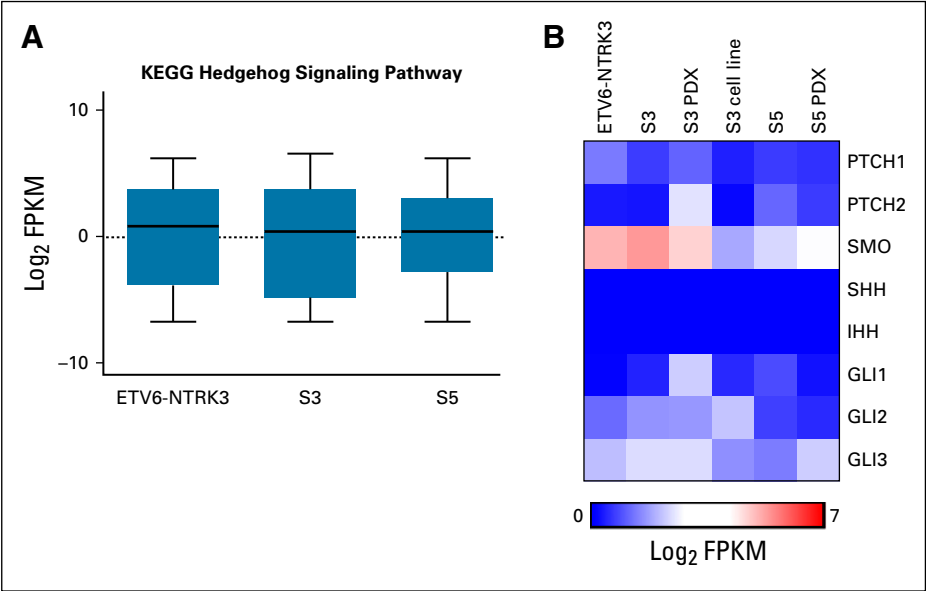


FIG A2. Hedgehog pathway gene expression. (A) Expression of genes in the KEGG Hedgehog signaling pathway gene set. (B) Heatmap of RNA-seq data showing expression of select genes essential to Hedgehog cellular signaling. PDX, patient-derived xenograft; S, surgery.

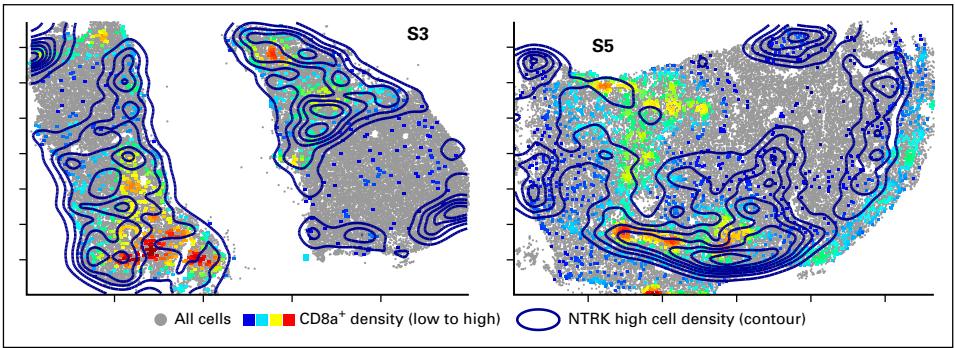


FIG A3. Colocalization of CD8a⁺ and TRK^{high} cells. Global distribution of cells staining highest for tropomyosin receptor kinase (TRK; contour map) and CD8a⁺ cells (heatmap, with red indicating higher cell density) in surgery (S) 3 and S5.

TABLE A1. Antibodies Used for t-CyCIF

Cycle No. and Ch/ Filter	Antibody Name	Target Protein	Vendor	Catalog No.	Clone	Conjugated Fluorophore
1						
488/FITC	pan-TRK	NTRK1/2/3	Abcam, Cambridge, United Kingdom	ab181560	EPR17341	n/a
555/Cy3	anti-CTD2	pCTD2(S2)	Active Motif, Carlsbad, CA	61084	3E10	n/a
647/Cy5	anti-CD20	CD20	DAKO, Santa Clara, CA	M07555	L26	n/a
2						
488/FITC	CD4-488	CD4	R&D Systems, Minneapolis, MN	FAB8165G	Polyclonal	Alexa Fluor 488
555/Cy3	CD3D-555	CD3D	Abcam	AB208514	EP4426	Alexa Fluor 555
647/Cy5	PD1-647	PD1	Abcam	AB201825	EPR4877 (2)	Alexa Fluor 647
3						
488/FITC	Ki67-488	Ki67	CST, Danvers, MA	11882	D3B5	Alexa Fluor 488
555/Cy3	FOXP3-570	FOXP3	eBioscience, Waltham, MA	41-4777-80	236A/E7	eFluor 570
647/Cy5	PDL1-647	PD-L1/ CD274	CST	15005	E1L3N	Alexa Fluor 647
4						
488/FITC	IBA1-488	IBA1	Abcam	ab195031	EPR6136(2)	Alexa Fluor 488
555/Cy3	CD68-PE	CD68	CST	79594	D4B9C	PE
647/Cy5	CD45-647	CD45	BioLegend, San Diego, CA	304020	HI30	Alexa Fluor 647
5						
488/FITC	anti-PTEN	PTEN	CST	9559	138G6	Zenon-488
555/Cy3	Keratin-570	pan-Keratin	eBioscience	41-9003-80	AE1/AE3	eFluor 570
647/Cy5	CD8a-660	CD8	eBioscience	50-0008-80	AMC908	eFluor 660
6						
488/FITC	p53-488	p53	CST	5429	7F5	Alexa Fluor 488
555/Cy3	pH3-555	pH3(S10)	CST	3475	D2C8	Alexa Fluor 555
647/Cy5	gH2ax-647	H2ax(S139)	CST	9720	20E3	Alexa Fluor 647
7						
488/FITC			Background			
555/Cy3			Background			
647/Cy5			Background			
8						
488/FITC	pS6(S240/ 244)-488	pS6(240/ 244)	CST	5018	D68F8	Alexa Fluor 488
555/Cy3	VEGFR2-PE	VEGFR2	CST	12634	D5B1	PE
647/Cy5	NGFR-647	NGFR/CD271	Abcam	AB195180	EP1039Y	Alexa Fluor 647

Abbreviations: Ch, channel; CST, Cell Signaling Technology; n/a, not applicable; PE, phycoerythrin; t-CyCIF, tissue-based cyclic immunofluorescence.